

Spin Light Emitting Diode Based on Exciton Fine Structure Tuning in Quantum Dots

A. V. Shumilin^{1,2}, T. S. Shamirzaev³, and D. S. Smirnov¹

¹*Ioffe Institute, 194021 St. Petersburg, Russia*

²*Complex Matter Department, Jozef Stefan Institute, Jamova 39, SI-1000 Ljubljana, Slovenia*

³*Rzhanov Institute of Semiconductor Physics, Siberian Branch of the Russian Academy of Sciences, 630090 Novosibirsk, Russia*



(Received 26 June 2023; accepted 17 January 2024; published 16 February 2024)

We propose a concept of quantum dot based light emitting diode that produces circularly polarized light without magnetic contacts due to the hyperfine interaction at the crossing of the exciton levels in a weak magnetic field. The electroluminescence circular polarization degree can reach 100%. The concept is compatible with the micropillar cavities, which allows for the generation of single circularly polarized photons. Second order photon correlation function includes information about the nuclear spin dynamics in the quantum dot, and the nuclear spin state can be purified by the quantum measurement backaction.

DOI: [10.1103/PhysRevLett.132.076202](https://doi.org/10.1103/PhysRevLett.132.076202)

Introduction.—The compact sources of circularly polarized light are strongly anticipated for the opto-spintronic applications in general and for the quantum information processing in particular [1,2]. The circularly polarized light can be obtained using the optical activity of bulk crystals, heterostructures [3–5], or organic molecules [6,7].

Much more compact devices exploit chiral vacuum electromagnetic modes, which can be created in chiral photonic crystals, using chiral metasurfaces [8–11], or exploiting a chiral design of heterostructures [12–14].

Even more compact and technologically simple sources of circularly polarized light are based on the spin polarization of the charge carriers involved in the light emission. For example, absorption of circularly polarized light leads to optical spin orientation and reemission of circularly polarized light provided the spin relaxation time is long enough [15]. For practical applications, the electrical spin injection is more favorable, and such sources of circularly polarized light are widely known as spin-light emitting diodes (LEDs) [16]. In spin-LEDs, the spin is injected to single or multiple quantum wells or quantum dots (QDs) from ferromagnetic contacts [17–24] or chiral environment, such as organic molecules [25,26]. Especially there is renewed interest in the studies of QDs nowadays [27].

We put forward an alternative concept of spin-LEDs that exploits the fine structure tuning of excitons in semiconductor QDs by magnetic field. In it, no ferromagnetic contacts are needed, the sense of the circular polarization of the electroluminescence (EL) is determined by a tiny magnetic field of the order of ten millitesla, and the size of the device can be much smaller than the light wavelength.

Tuning of the exciton fine structure by magnetic field can lead to the so-called dynamic electron spin polarization effect, i.e., appearance of a large electron spin polarization in nonequilibrium conditions due to the electron-nuclear flip-flops, which can be used to produce circularly

polarized light. This effect was first described and observed in momentum indirect type-I (In, Al)As/AlAs QDs [28], which show long spin relaxation times up to milliseconds at zero magnetic field. Later, the dynamic electron spin polarization effect was described theoretically [29] and observed experimentally [30] for moiré quantum dots in twisted transition metal dichalcogenides heterobilayers. It was also theoretically shown to take place under electric current flow in organic semiconductor molecules [31], which are often used for LEDs [32,33]. The clear analogies can be observed with the effects of nuclear self polarization [34], magnetocircular photoluminescence [35], and chemically induced dynamic electron polarization [36,37].

We describe QD-based spin-LEDs, which are based on the dynamic electron spin polarization effect. Such structures are compatible with the micropillar cavities [38–41], which can be used to enhance the emission directionality and produce single photons [42,43]. In combination, this allows for the generation of single circularly polarized photons by electric pulses and promises to find an important application in quantum communications and photon-based computations.

Model.—The device under consideration basically represents a QD based LED in external magnetic field with electrical injection of electrons and holes from *n*-type and *p*-type contacts to intermediate intrinsic layer with self-assembled QDs, see Fig. 1(a). The QDs are assumed to be made of GaAs-type semiconductors and to be small enough so that only the first size quantized levels of electron and hole in QDs can be considered (and we neglect the possible valley degeneracy). The relevant temperatures are below the liquid nitrogen temperature. We denote the electron and hole capture rates to an empty QD as γ_e and γ_h , respectively. The single particle states are Kramers degenerate with respect to the electron spin $S_z = \pm 1/2$ and the heavy hole spin $J_z = \pm 3/2$. When a QD captures both an electron

and a hole, an exciton forms. It can recombine radiatively with the rate γ_0 in the bright spin state, according to the optical selection rules [15]: $S_z = \mp 1/2$ electron can recombine with $J_z = \pm 3/2$ hole only emitting circularly polarized σ^\pm photon, respectively.

We consider the limit of

$$\gamma_0 \gg \gamma_e \gg \gamma_h \quad (1)$$

and assume the strong Coulomb interaction, which forbids occupancy of a QD by two electrons without a hole. The possible transitions between QD states are shown in Fig. 1(b): Starting from the empty QD state (\emptyset), first, an electron with spin-up or spin-down is captured by the QD (blue dashed arrows) because of the assumptions of much slower hole capture rate. Then due to the Coulomb blockade only a hole can be captured with the rate γ_h (red dotted arrows). Afterwards, if the bright exciton is formed, it quickly radiatively recombines (yellow solid wavy arrows). If the dark exciton with parallel electron and hole spins is formed, there are two options: (i) It can recombine radiatively [yellow dashed wavy arrows in Fig. 1(b)] due to the mixing of bright and dark excitonic states by the

hyperfine interaction. The corresponding recombination rate γ_\pm is small ($\sim \gamma_e$) and depends on the spin of the hole in the exciton $J_z = \pm 3/2$. (ii) A second electron with the opposite spin can be captured with the rate $\gamma_e/2$. In the latter case, the singlet trion forms and quickly recombines radiatively with the rate γ_0 (dark cyan wavy arrows). Then a single electron remains in the QD. The interplay between these two options produces the circular polarization of the emitted light, as we show below.

The exciton spin dynamics is driven by the electron hyperfine interaction, exchange interaction, and external magnetic field \mathbf{B} . The Bloch equation for the electron spin \mathbf{S} reads [44]: $d\mathbf{S}/dt = (g_e\mu_B/\hbar)\mathbf{B}_{\text{tot}} \times \mathbf{S}$, where g_e is the electron g factor, μ_B is the Bohr magneton, and $\mathbf{B}_{\text{tot}} = \mathbf{B} + \mathbf{B}_n + (2J_z/3)\mathbf{B}_{\text{exch}}\mathbf{e}_z$ is the total effective magnetic field, which includes the exchange field $\pm\mathbf{B}_{\text{exch}}$ along the z axis [45], and the Overhauser field \mathbf{B}_n of randomly oriented nuclear spins. The nuclear spin fluctuations produce ‘‘frozen’’ Overhauser field with the Gaussian probability distribution function $\propto \exp(-B_n^2/\Delta_B^2)$, where Δ_B characterizes the dispersion [46]. In the limit of fast electron spin precession, we obtain the recombination rates of the dark excitons [47]:

$$\gamma_\pm = \gamma_0 \frac{B_{n,x}^2 + B_{n,y}^2}{4(B \pm B_{\text{exch}})^2}. \quad (2)$$

We note that the mixing can be provided by the tilted external magnetic field as well.

The QD is occupied most of the time with a single electron, so its state can be characterized by the two occupancies $p_{\uparrow/\downarrow}$ of spin-up and spin-down states. From Fig. 1(b) one can see that the rates of the trion recombination with emission of σ^\pm photons are given by

$$I_\pm^{\text{tr}} = \frac{p_{\uparrow/\downarrow}\gamma_e\gamma_h/4}{\gamma_e/2 + \gamma_\pm}. \quad (3)$$

At the same time, the rates of σ^\pm photon emission by excitons are $I_\pm^{\text{ex}} = \gamma_h/2 - I_\pm^{\text{tr}}$, so the total EL is unpolarized, while exciton and trion ELs are polarized oppositely.

The kinetic equations for the occupancies read

$$\frac{dp_{\uparrow/\downarrow}}{dt} = \pm \frac{1}{2} [\gamma_h(p_\downarrow - p_\uparrow) + I_+^{\text{tr}} - I_-^{\text{tr}}]. \quad (4)$$

From these equations we find the intensities of the exciton and trion EL in the steady state $\langle I^{\text{ex/tr}} \rangle = \langle I_+^{\text{ex/tr}} + I_-^{\text{ex/tr}} \rangle$, their polarizations $P_{\text{ex/tr}} = \langle I_+^{\text{ex/tr}} - I_-^{\text{ex/tr}} \rangle / \langle I^{\text{ex/tr}} \rangle$, and the electron spin polarization $P_e = \langle p_\uparrow - p_\downarrow \rangle$, where the angular brackets denote the averaging over the random Overhauser field. Generally, the polarizations are determined by the two dimensionless parameters B/B_{exch} and $\mathcal{R} = \gamma_e B_{\text{exch}}^2 / (\gamma_0 \Delta_B^2)$.

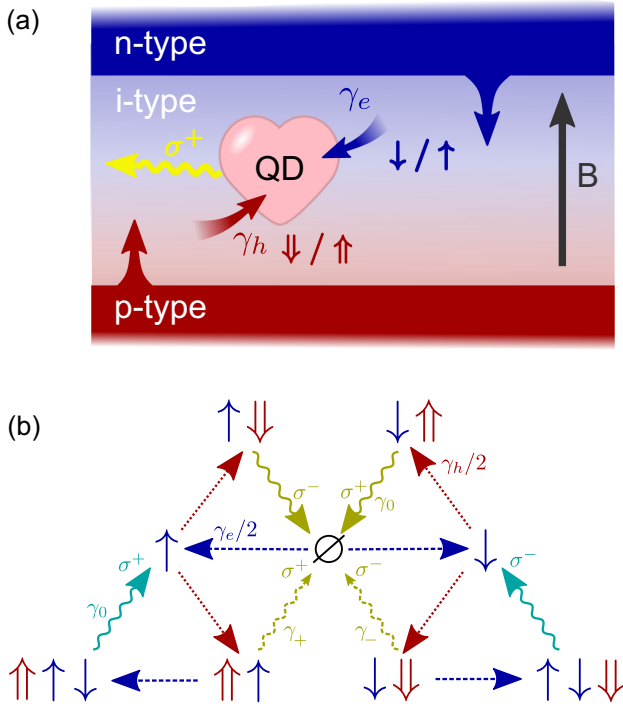


FIG. 1. (a) Electrical injection of electrons (blue) and holes (red) to a QD (heart of the device), which emits circularly polarized light (yellow). (b) Transitions between different QD states. Blue and red solid arrows denote electron and hole spins, \emptyset is the empty QD state, blue dashed and red dotted arrows denote capture of electrons and holes, respectively, yellow and dark cyan wavy arrows are the exciton and trion radiative recombinations, which obey the optical selection rules.

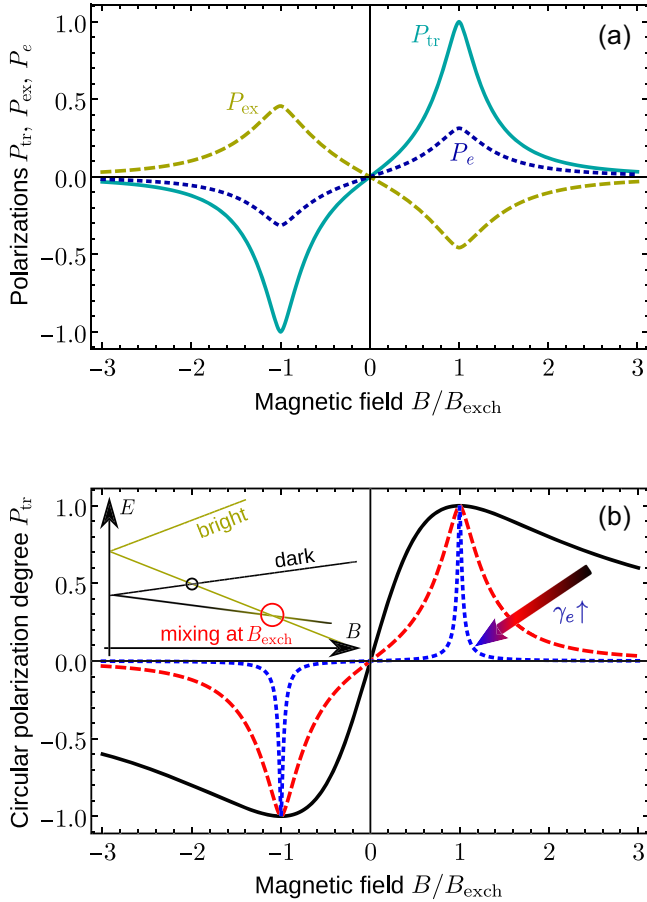


FIG. 2. (a) Polarizations of trion EL (solid dark cyan line), exciton EL (yellow dashed line), and an electron (blue dotted line) for $\mathcal{R} = 2.5$. (b) Polarization of trion EL for increasing electron injection rate: $\mathcal{R} \rightarrow 0$ (black solid line), $\mathcal{R} = 2.5$ (red dashed line), and $\mathcal{R} = 250$ (blue dotted line). The inset shows the splitting of bright and dark excitonic states in magnetic field. At the level crossing shown by the red circle ($B = B_{exch}$) the polarizations are the largest.

Results.—We show the polarization degrees of trion and exciton EL and of the electron spin in Fig. 2(a) as functions of the magnetic field. These functions are odd in agreement with the time reversal symmetry and reach the largest values at $|B| = B_{exch}$ (we assume $B_{exch} > 0$, which corresponds to the negative electron g factor). This can be understood from the inset in Fig. 2(b), which shows the splitting of the exciton levels in magnetic field. At $B = \pm B_{exch}$ the levels of a bright and a dark exciton with the same hole spin cross (red circle in the inset), so their mixing due to the hyperfine interaction is the strongest. Note that there is also another level crossing shown by a small black circle in the inset in Fig. 2(b), but the corresponding mixing between bright and dark states requires hole spin flips, which we neglect [47] due to p -type hole Bloch wave functions [48].

The electron spin polarization cannot exceed 1/3, the exciton EL polarization is generally smaller than 1/2,

but the trion EL polarization can reach 100%. So for the rest of the Letter we focus on it. We note that it is well separated from the exciton EL by the trion binding energy, which allows one to easily select it experimentally. Figure 2(b) shows the dependence of the trion EL polarization on the magnetic field, which can have qualitatively different shape. Provided $\mathcal{R} \ll 1$, we obtain $P_{tr} = 2BB_{exch}/(B^2 + B_{exch}^2)$ [47]. So this dependence is broad and slowly decays with increase of the magnetic field, as shown by the black solid line in Fig. 2(b). With increase of \mathcal{R} , the narrow resonances appear in the polarization at $B = \pm B_{exch}$, as shown by the red dashed and blue dotted lines. In the limit of $\mathcal{R} \gg 1$, the dynamic electron spin polarization effect basically reduces to the magnetic circular polarization of exciton photoluminescence effect [35].

Single photon source.—The self-assembled QDs can be easily embedded in micropillar cavities to enhance light-matter interaction and to increase directionality of the emission [38–41]. A sketch of the device is shown in Fig. 3(a). Electrons and holes can be injected electrically into the single QD and an additional contact to intrinsic layer can allow one to change the rates γ_e and γ_h independently. The electron hole recombination at the level crossing ($B = B_{exch}$) produces circularly polarized light, and one can tune the microcavity resonance frequency to select the emission at the trion resonance frequency and suppress another frequencies.

The counting statistics of the emitted photons can be described on the basis of Eqs. (3) and (4). For $\mathcal{R} \gg 1$, the level crossing is described by $\gamma_- \gg \gamma_e \gg \gamma_+$, and the corresponding transitions between QD states are shown in Fig. 3(b). The simplified kinetic equations read $d p_{\uparrow/\downarrow}/dt = \pm \gamma_h (p_{\downarrow}/2 - p_{\uparrow}/4)$, they are valid at the slowest timescale $\sim 1/\gamma_h$. After the trion recombination with emission of σ^+ photon, the system is left in the electron spin-up state. The next photon cannot be emitted immediately after this, so the emitted photons are antibunched at the timescale $\sim 1/\gamma_0$. However, at the longer timescale, the increased occupation of the electron spin-up state increases the probability of the second σ^+ photon emission relative to the steady state. This leads to the bunching of photons emitted from the device at the timescale $\sim 1/\gamma_h$. The second order photon correlation function $g_{s.s.}^{(2)}(\tau) = \langle I^{tr}(t)I^{tr}(t+\tau) \rangle / \langle I^{tr}(t) \rangle^2$ is shown in Fig. 3(c) and decreases from 1.5 to 1. The antibunching at the short timescale is not shown.

The antibunching at the long timescale can be achieved by applying electrical pulses. Thus, we consider a small constant hole capture rate γ_h and a pulsed electron capture rate γ_e during the pulse duration T . In this case, the QD is initially charged with a single hole with the unpolarized spin. After beginning of the pulse, satisfying Eq. (1), the EL appears. A single photon can be emitted immediately after injection of an electron. However, the second photon

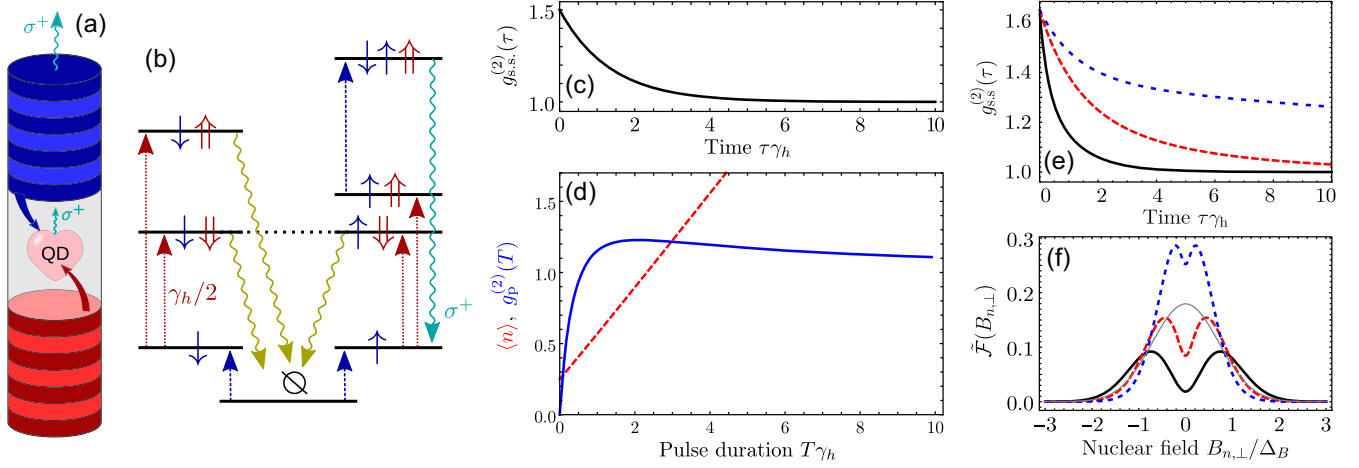


FIG. 3. (a) Sketch of a QD micropillar cavity with electron and hole injection. (b) Energy diagram of the QD states and transitions corresponding to Fig. 1(b) in the resonant approximation. (c) Second order photon correlation function in the steady state. (d) EL intensity (red dashed line) and second order photon correlation function (blue solid line) under pulsed excitation as functions of the pulse duration. (e) The same as in (c) for $\mathcal{R} = 1/8$, $B = B_{\text{exch}}/2$ and with account for the nuclear spin relaxation time $\tau_s^n = 1/\gamma_h$ (black solid line), $10/\gamma_h$ (red dashed line), and $100/\gamma_h$ (blue dotted line). (f) Purified nuclear field distribution functions $\tilde{\mathcal{F}}(B_{n,\perp})$ after detection of $N = 0$ (black solid line), 1 (red dashed line), and 2 (blue dotted line) photons during the time $6.23/\gamma_h$ calculated numerically for the same \mathcal{R} and B as in (e) [47]. The gray thin line shows the equilibrium distribution function.

cannot be emitted before another hole is captured with the slow rate γ_h . As a result, the electric pulses produce strongly antibunched EL when $T \lesssim 1/\gamma_h$, even if their length is much longer than the radiative recombination time and the inverse electron capture rate.

The photon statistics is described by the same kinetic equations and the photon correlation function in the pulsed regime is given by $g_p^{(2)}(T) = \langle n(n-1) \rangle / \langle n \rangle^2$, where n is the number of emitted photons and the angular brackets denote the quantum statistical averaging. It is shown in Fig. 3(d) by the blue solid line as a function of the electrical pulse duration (an explicit expression for it is given in the Supplemental Material [47]). One can see a perfect antibunching $g_p^{(2)}(0) = 0$ in the limit of the short pulses. Most importantly, the EL remains antibunched [$g_p^{(2)}(T) < 1$] even for the long pulses with $T < 0.6/\gamma_h$ in contrast to the steady state EL.

An important characteristic of the device along with the circular polarization degree is its brightness [26,49–51]. In our case, it is limited by the hole capture rate γ_h , which should be smaller than the radiative decay rate γ_0 . As a result, one can expect the single photon generation rates in the megahertz range.

Manipulating nuclear spin state.—The interplay between dark exciton radiative recombination and electron capture becomes important beyond the resonant approximation, $B \approx B_{\text{exch}}$, or for small \mathcal{R} . Then the nuclear spin fluctuations determine the intensity of EL. As a result, the nuclear spin dynamics contributes to the photon correlation function by increasing the bunching in the steady state and introducing an additional timescale. This is illustrated in Fig. 3(e), where we account for the nuclear spin relaxation

time τ_s^n on the basis of the Fokker-Planck equation for the nuclear spin distribution function for $B = B_{\text{exch}}/2$ [47]. One can see that it produces a longer tail in the photon correlation function. Generally, the nuclear spin dynamics in small magnetic fields is poorly investigated, and this effect provides a unique opportunity to access it directly in the experiment.

Moreover, photon detection modifies the collective nuclear spin state and reduces its entropy due to the quantum measurement backaction, as demonstrated in Ref. [52] for a different system. The distribution functions of transverse nuclear spin components $\mathcal{F}(B_{n,\perp})$ purified by the selective measurement of 0, 1, and 2 photons during the time $6.23/\gamma_h$ is shown in Fig. 3(f). The equilibrium distribution function is shown by the thin gray line for comparison. Its modification allows one to prepare squeezed nuclear spin states [53] with smaller or larger transverse fluctuations.

Discussion.—The dynamic electron spin polarization effect allows for the generation of circularly polarized light by QDs with the sizes of the order of 10 nm, which can be directly integrated into the optical waveguides. We also stress that in our concept of spin LEDs no magnetic components are required, and the circularly polarized EL is produced in a small magnetic field $B = B_{\text{exch}}$. The possible parameters of the device can be as follows [28,44,54]: $B_{\text{exch}} = 15$ mT, $\Delta_B = 3$ mT, $\gamma_0 = 1$ ns $^{-1}$, $\gamma_e = 10$ μ s $^{-1}$, $\gamma_h = 1$ μ s $^{-1}$, the circular polarization degree for them exceeds 90% [47]. We note, however, that the tunneling rates can be tuned in a wide range. A small magnetic field can be easily switched to control the sense of EL circular polarization.

In conclusion, we have put forward a concept of spin-LEDs based on the effect of dynamic electron spin polarization due to the exciton fine structure tuning by magnetic field and electron hyperfine interaction. In this concept, the spin-LEDs do not require magnetic or chiral elements and can produce completely circularly polarized light, having a size smaller than the wavelength. By embedding a single QD in a zero dimensional microcavity one can get a device, which produces single circularly polarized photons with variable helicity.

We acknowledge the Foundation for the Advancement of Theoretical Physics and Mathematics “BASIS.” The development of the device structure by T. S. Sh. was supported by the Russian Science Foundation Grant No. 22-12-00022. The description of single photon EL and measurement backaction by D. S. S. was supported by the Russian Science Foundation Grant No. 23-12-00142.

-
- [1] M. Atatüre, D. Englund, N. Vamivakas, S.-Y. Lee, and J. Wrachtrup, Material platforms for spin-based photonic quantum technologies, *Nat. Rev. Mater.* **3**, 38 (2018).
- [2] H. Hübener, U. D. Giovannini, C. Schäfer, J. Andberger, M. Ruggenthaler, J. Faist, and A. Rubio, Engineering quantum materials with chiral optical cavities, *Nat. Mater.* **20**, 438 (2020).
- [3] L. V. Kotova, A. V. Platonov, V. N. Kats, V. P. Kochereshko, S. V. Sorokin, S. V. Ivanov, and L. E. Golub, Optical activity of quantum wells, *Phys. Rev. B* **94**, 165309 (2016).
- [4] A. V. Poshakinskiy, D. R. Kazanov, T. V. Shubina, and S. A. Tarasenko, Optical activity in chiral stacks of 2D semiconductors, *Nanophotonics* **7**, 753 (2018).
- [5] J. Michl, C. C. Palekar, S. A. Tarasenko, F. Lohof, C. Gies, M. von Helversen, R. Sailus, S. Tongay, T. Taniguchi, K. Watanabe, T. Heindel, B. Rosa, M. Rödel, T. Shubina, S. Höfling, S. Reitzenstein, C. Anton-Solanas, and C. Schneider, Intrinsic circularly polarized exciton emission in a twisted van der Waals heterostructure, *Phys. Rev. B* **105**, L241406 (2022).
- [6] N. Y. Ha, Y. Ohtsuka, S. M. Jeong, S. Nishimura, G. Suzuki, Y. Takanishi, K. Ishikawa, and H. Takezoe, Fabrication of a simultaneous red-green-blue reflector using single-pitched cholesteric liquid crystals, *Nat. Mater.* **7**, 43 (2007).
- [7] J. Pu, W. Zhang, H. Matsuoka, Y. Kobayashi, Y. Takaguchi, Y. Miyata, K. Matsuda, Y. Miyauchi, and T. Takenobu, Room-temperature chiral light-emitting diode based on strained monolayer semiconductors, *Adv. Mater.* **33**, 2100601 (2021).
- [8] K. Konishi, M. Nomura, N. Kumagai, S. Iwamoto, Y. Arakawa, and M. Kuwata-Gonokami, Circularly polarized light emission from semiconductor planar chiral nanostructures, *Phys. Rev. Lett.* **106**, 057402 (2011).
- [9] N. Shitrit, I. Yulevich, E. Maguid, D. Ozeri, D. Veksler, V. Kleiner, and E. Hasman, Spin-optical metamaterial route to spin-controlled photonics, *Science* **340**, 724 (2013).
- [10] Z. Li, C. Liu, X. Rong, Y. Luo, H. Cheng, L. Zheng, F. Lin, B. Shen, Y. Gong, S. Zhang, and Z. Fang, Tailoring MoS₂ valley-polarized photoluminescence with super chiral near-field, *Adv. Mater.* **30**, 1801908 (2018).
- [11] A. A. Maksimov, E. V. Filatov, I. I. Tartakovskii, V. D. Kulakovskii, S. G. Tikhodeev, C. Schneider, and S. Höfling, Circularly polarized laser emission from an electrically pumped chiral microcavity, *Phys. Rev. Appl.* **17**, L021001 (2022).
- [12] J. Lin, J. P. B. Mueller, Q. Wang, G. Yuan, N. Antoniou, X.-C. Yuan, and F. Capasso, Polarization-controlled tunable directional coupling of surface plasmon polaritons, *Science* **340**, 331 (2013).
- [13] F. Spitzer, A. N. Poddubny, I. A. Akimov, V. F. Sapega, L. Klompmaker, L. E. Kreilkamp, L. V. Litvin, R. Jede, G. Karczewski, M. Wiater, T. Wojtowicz, D. R. Yakovlev, and M. Bayer, Routing the emission of a near-surface light source by a magnetic field, *Nat. Phys.* **14**, 1043 (2018).
- [14] X. Yin, J. Jin, M. Soljačić, C. Peng, and B. Zhen, Observation of topologically enabled unidirectional guided resonances, *Nature (London)* **580**, 467 (2020).
- [15] E. L. Ivchenko, *Optical Spectroscopy of Semiconductor Nanostructures* (Alpha Science, Harrow, United Kingdom, 2005).
- [16] M. Holub and P. Bhattacharya, Spin-polarized light-emitting diodes and lasers, *J. Phys. D* **40**, R179 (2007).
- [17] Y. Ohno, D. K. Young, B. Beschoten, F. Matsukura, H. Ohno, and D. D. Awschalom, Electrical spin injection in a ferromagnetic semiconductor heterostructure, *Nature (London)* **402**, 790 (1999).
- [18] R. Fiederling, M. Keim, G. Reuscher, W. Ossau, G. Schmidt, A. Waag, and L. W. Molenkamp, Injection and detection of a spin-polarized current in a light-emitting diode, *Nature (London)* **402**, 787 (1999).
- [19] Y. Chye, M. E. White, E. Johnston-Halperin, B. D. Gerardot, D. D. Awschalom, and P. M. Petroff, Spin injection from (Ga,Mn)As into InAs quantum dots, *Phys. Rev. B* **66**, 201301(R) (2002).
- [20] X. Jiang, R. Wang, R. M. Shelby, R. M. Macfarlane, S. R. Bank, J. S. Harris, and S. S. P. Parkin, Highly spin-polarized room-temperature tunnel injector for semiconductor spintronics using MgO(100), *Phys. Rev. Lett.* **94**, 056601 (2005).
- [21] K. Hamaya, M. Kitabatake, K. Shibata, M. Jung, S. Ishida, T. Taniyama, K. Hirakawa, Y. Arakawa, and T. Machida, Spin-related current suppression in a semiconductor quantum dot spin-diode structure, *Phys. Rev. Lett.* **102**, 236806 (2009).
- [22] J.-Y. Chen, T.-M. Wong, C.-W. Chang, C.-Y. Dong, and Y.-F. Chen, Self-polarized spin-nanolasers, *Nat. Nanotechnol.* **9**, 845 (2014).
- [23] N. Nishizawa, K. Nishibayashi, and H. Munekata, Pure circular polarization electroluminescence at room temperature with spin-polarized light-emitting diodes, *Proc. Natl. Acad. Sci. U.S.A.* **114**, 1783 (2017).
- [24] M. Lindemann, G. Xu, T. Pusch, R. Michalzik, M. R. Hofmann, I. Žutić, and N. C. Gerhardt, Ultrafast spin-lasers, *Nature (London)* **568**, 212 (2019).
- [25] Y. Yang, R. C. da Costa, D.-M. Smilgies, A. J. Campbell, and M. J. Fuchter, Induction of circularly polarized electroluminescence from an achiral light-emitting polymer via a chiral small-molecule dopant, *Adv. Mater.* **25**, 2624 (2013).

- [26] Y.-H. Kim, Y. Zhai, H. Lu, X. Pan, C. Xiao, E. A. Gaulding, S. P. Harvey, J. J. Berry, Z. V. Vardeny, J. M. Luther, and M. C. Beard, Chiral-induced spin selectivity enables a room-temperature spin light-emitting diode, *Science* **371**, 1129 (2021).
- [27] K. Yu and K. S. Schanze, Commemorating The Nobel Prize in Chemistry 2023 for the Discovery and Synthesis of Quantum Dots, ACS Central Science (2023).
- [28] D. S. Smirnov, T. S. Shamirzaev, D. R. Yakovlev, and M. Bayer, Dynamic polarization of electron spins interacting with nuclei in semiconductor nanostructures, *Phys. Rev. Lett.* **125**, 156801 (2020).
- [29] D. S. Smirnov, Dynamic valley polarization in moiré quantum dots, *Phys. Rev. B* **104**, L241401 (2021).
- [30] X. Wang, C. Xiao, H. Park, J. Zhu, C. Wang, T. Taniguchi, K. Watanabe, J. Yan, D. Xiao, D. R. Gamelin, W. Yao, and X. Xu, Light-induced ferromagnetism in moiré superlattices, *Nature (London)* **604**, 468 (2022).
- [31] A. V. Shumilin, Dynamic spin polarization in organic semiconductors with intermolecular exchange interaction, *Phys. Rev. B* **105**, 104206 (2022).
- [32] S. R. Forrest, The path to ubiquitous and low-cost organic electronic appliances on plastic, *Nature (London)* **428**, 911 (2004).
- [33] Q. Wei, N. Fei, A. Islam, T. Lei, L. Hong, R. Peng, X. Fan, L. Chen, P. Gao, and Z. Ge, Small-molecule emitters with high quantum efficiency: Mechanisms, structures, and applications in OLED devices, *Adv. Opt. Mater.* **6**, 1800512 (2018).
- [34] M. I. Dyakonov and V. I. Perel, Dynamic nuclear self-polarization, *JETP Lett.* **16**, 398 (1972).
- [35] E. L. Ivchenko, Magnetic circular polarization of exciton photoluminescence, *Phys. Solid State* **60**, 1514 (2018).
- [36] J. B. Pedersen and J. H. Freed, Theory of chemically induced dynamic electron polarization. I, *J. Chem. Phys.* **58**, 2746 (1973).
- [37] U. E. Steiner and T. Ulrich, Magnetic field effects in chemical kinetics and related phenomena, *Chem. Rev.* **89**, 51 (1989).
- [38] N. Somaschi, V. Giesz, L. De Santis, J. C. Loredó, M. P. Almeida, G. Hornecker, S. L. Portalupi, T. Grange, C. Anton, J. Demory, C. Gomez, I. Sagnes, N. D. Lanzillotti-Kimura, A. Lemaitre, A. Auffeves, A. G. White, L. Lanco, and P. Senellart, Near-optimal single-photon sources in the solid state, *Nat. Photonics* **10**, 340 (2016).
- [39] S. Unsleber, Y.-M. He, S. Gerhardt, S. Maier, C.-Y. Lu, J.-W. Pan, N. Gregersen, M. Kamp, C. Schneider, and S. Höfling, Highly indistinguishable on-demand resonance fluorescence photons from a deterministic quantum dot micropillar device with 74% extraction efficiency, *Opt. Express* **24**, 8539 (2016).
- [40] A. I. Galimov, M. V. Rakhlin, G. V. Klimko, Y. M. Zadiranov, Y. A. Guseva, S. I. Troshkov, T. V. Shubina, and A. A. Toropov, Source of indistinguishable single photons based on epitaxial InAs/GaAs quantum dots for integration in quantum computing schemes, *JETP Lett.* **113**, 252 (2021).
- [41] N. Tömm, A. Javadi, N. O. Antoniadis, D. Najer, M. C. Löbl, A. R. Korsch, R. Schott, S. R. Valentin, A. D. Wieck, A. Ludwig, and R. J. Warburton, A bright and fast source of coherent single photons, *Nat. Nanotechnol.* **16**, 399 (2021).
- [42] A. J. Bennett, D. C. Unitt, P. See, A. J. Shields, P. Atkinson, K. Cooper, and D. A. Ritchie, Microcavity single-photon-emitting diode, *Appl. Phys. Lett.* **86**, 181102 (2005).
- [43] T. Heindel, C. Schneider, M. Lermer, S. H. Kwon, T. Braun, S. Reitzenstein, S. Höfling, M. Kamp, and A. Forchel, Electrically driven quantum dot-micropillar single photon source with 34% overall efficiency, *Appl. Phys. Lett.* **96**, 011107 (2010).
- [44] T. S. Shamirzaev, A. V. Shumilin, D. S. Smirnov, J. Rautert, D. R. Yakovlev, and M. Bayer, Dynamic polarization of electron spins in indirect band gap (In, Al)As/AlAs quantum dots in a weak magnetic field: Experiment and theory, *Phys. Rev. B* **104**, 115405 (2021).
- [45] G. V. Astakhov, A. V. Koudinov, K. V. Kavokin, I. S. Gakis, Y. G. Kusrayev, W. Ossau, and L. W. Molenkamp, Exciton spin decay modified by strong electron-hole exchange interaction, *Phys. Rev. Lett.* **99**, 016601 (2007).
- [46] I. A. Merkulov, A. L. Efros, and M. Rosen, Electron spin relaxation by nuclei in semiconductor quantum dots, *Phys. Rev. B* **65**, 205309 (2002).
- [47] See Supplemental Material at <http://link.aps.org/supplemental/10.1103/PhysRevLett.132.076202> for (i) details of the derivation and numerical solution of the kinetic equations, (ii) calculation of the second order correlation functions in the steady state and under pulsed excitation, (iii) description of the role of nuclear spin dynamics and nuclear spin bath purification.
- [48] M. M. Glazov, *Electron & Nuclear Spin Dynamics in Semiconductor Nanostructures* (Oxford University Press, Oxford, 2018).
- [49] L. Grenet, M. Jamet, P. Noé, V. Calvo, J.-M. Hartmann, L. E. Nistor, B. Rodmacq, S. Auffret, P. Warin, and Y. Samson, Spin injection in silicon at zero magnetic field, *Appl. Phys. Lett.* **94**, 032502 (2009).
- [50] F. Cadiz, A. Djeflal, D. Lagarde, A. Balocchi, B. Tao, B. Xu, S. Liang, M. Stoffel, X. Devaux, H. Jaffres, J.-M. George, M. Hehn, S. Mangin, H. Carrere, X. Marie, T. Amand, X. Han, Z. Wang, B. Urbaszek, Y. Lu, and P. Renucci, Electrical initialization of electron and nuclear spins in a single quantum dot at zero magnetic field, *Nano Lett.* **18**, 2381 (2018).
- [51] K. Etou, S. Hiura, S. Park, K. Sakamoto, J. Takayama, A. Subagyo, K. Sueoka, and A. Murayama, Room-temperature spin-transport properties in an In_{0.5}Ga_{0.5}As quantum dot spin-polarized light-emitting diode, *Phys. Rev. Appl.* **16**, 014034 (2021).
- [52] D. B. R. Dasari, S. Yang, A. Chakrabarti, A. Finkler, G. Kurizki, and J. Wrachtrup, Anti-Zeno purification of spin baths by quantum probe measurements, *Nat. Commun.* **13**, 7527 (2022).
- [53] M. Kitagawa and M. Ueda, Squeezed spin states, *Phys. Rev. A* **47**, 5138 (1993).
- [54] T. S. Shamirzaev, A. V. Shumilin, D. S. Smirnov, D. Kudlacik, S. V. Nekrasov, Yu. G. Kusrayev, D. R. Yakovlev, and M. Bayer, Optical orientation of excitons in a longitudinal magnetic field in indirect-band-gap (In, Al)As/AlAs quantum dots with Type-I band alignment, *MDPI Nanomater.* **13**, 729 (2023).